Relative Magnetic Position and Rotation Sensor Assisted Dual-Foot Pedestrian Dead Reckoning

THESIS

Jenario Johnson

AFIT-ENG-MS-20-90210

DEPARTMENT OF THE AIR FORCE
AIR UNIVERSITY

AIR FORCE INSTITUTE OF TECHNOLOGY

Wright-Patterson Air Force Base, Ohio

AFIT-ENG-MS-20-90210

Relative Magnetic Position and Rotation Sensor Assisted Dual-Foot Pedestrian

Dead Reckoning

THESIS

Presented to the Faculty

Department of Electrical and Computer Engineering

Graduate School of Engineering and Management

Air Force Institute of Technology

Air University

Air Education and Training Command

in Partial Fulfillment of the Requirements for the

Degree of Master of Science in Electrical Engineering

Jenario Johnson, B.S.E.E.

March 24, 20222

Relative Magnetic Position and Rotation Sensor Assisted Dual-Foot Pedestrian

Dead Reckoning

THESIS

Jenario Johnson, B.S.E.E.

Committee Membership:

Clark Taylor, Ph.D
Chair

Meir Pachter, Ph.D
Member

Maj Joseph Curro, Ph.D
Member

AFIT-ENG-MS-20-90210

Abstract

Pedestrian Dead Reckoning (PDR) navigation systems attepmting to estimate a person's position based on an inertial measurement unit (IMU), must incorporate ways to account for the errors associated with IMUs, especially the drift errors. This research investigated the use of an alternative magnetic field sensor to measure relative position and orientation between the feet, coupled with foot-mounted IMUs, to capture pedestrian motion, and provide an algorithm and rationale for reducing the error associated with usage of the IMUs alone.

A two-phase approach was used to carry out this contribution. Using commercial grade IMUs, the pedestrian navigation system uses a Kalman filter with a Zero Velocity Update (ZUPT) measurement to form the first phase, and baseline, of the approach. The second phase investigated the inclusion of relative IMU measurements from the alternating field magnetic sensor. The first measurement used the position measurements of the magnetic sensors to create a foot-to-foot ranging measurement. The second measurement used the orientation measurements of the magnetic sensors to create a relative rotational measurement between the IMUs.

Results show substantial improvement of the body-worn IMU-based pedestrian navigation by incorporating the foot-to-foot ranging measurements. Further, there is improved accuracy of the baseline implementation with the use of the relative rotation measurements from the magnetic sensor, but not as much compared to the ranging measurements.

Table of Contents

List of Figures

List of Tables

Relative Magnetic Position and Rotation Sensor Assisted Dual-Foot Pedestrian
Dead Reckoning

I. Introduction

1.1   Motivation

Capturing human motion has many implications to the development of several
technologies and fields from animation to sports, medical, gaming, and much more.
Human motion capture seeks to harness our physical movement in a digital framework
to enhance our operation in these fields. In pedestrian navigation applications, human
bipedal movement can be used as a source of data for tracking our movement from one
place to another. Using this pedestrian motion, wearable technologies seek to not only
enhance our physical experiences, but also capitalize on these unique biometrics and
biomechanics. This two-way relationship of using body-worn technology to optimize
pedestrian navigation systems and using our bodies to enhance these systems' ability
to estimate position is a fundamental characteristic of IMU-based pedestrian naviga-
tion. Wearable technologies in the context of human navigation have this benefit in
terms of capturing, and quantifying, useful aspects of our movement.

Many techniques have been introduced in this space to capitalize on our natural
gait patterns to inform these navigation systems of what the data is representing and
what it means for our positional tracking. Many Pedestrian Navigation System (PNS)
also have the benefit of being self-contained. In this aspect, these systems can capture
our movement without any interaction with devices, or signals, not on the body [1].
Dependent PNS applications may use technologies such as Global Navigation Satellite

System (GNSS), Wireless Local Area Network (WLAN), and Bluetooth Low Energy (BLE). These technologies can become obstructed by enviornmental objects, limiting their applications. Unlike dependent PNS systems, self-contained applications virtually eliminate the possibility of interference. Pedestrian navigation makes wearable sensors, especially IMUs, attractive for self-contained applications because they can operate when other popular forms of navigation may be limited. Despite these useful features, wearable sensors, as with any real sensor, has error. These error include bias, scale factor and drift.

1.2 Research Problem and Justification

In the case of IMU-based PNS applications, the IMUs are affected by errors such as drift. Drift error is an effect of the friction from the moving parts within the IMUs, temperature, and the dielectric charging [2] [3]. These factors cause the output to drift over time, eventually dominating IMU's outputs. Higher quality IMUs, such as those used in Avionics systems mitigate the drift effects by using high-precision bearings and lubricants [2]. This grade of IMUs are usually larger, heavier, and more expensive, but do limit drift accumulation to several hours [1].

Consideration must be given to the size, weight, power, and cost, or SWaP-C of IMUs, when designing pedestrian navigation solutions with body-worn IMUs. Consumer-grade IMUs such as those integrated into smartphones, are low-cost and come in a small size. This grade of IMUs, has the trade-off of having poor performance characteristics compared to higher quality IMUs. Despite this low-quality, consumer-grade IMUs have become a standard for pedestrian tracking due to the small size, relatively low cost, and wide usage.

Robust pedestrian navigation systems based on the IMU have been introduced resolve the accumulating drift error of consumer-grade IMUs. One grouping of tech-

niques that seek to reduce these errors focus on recognizing patterns in human motion. These patterns are aspects of the gait that can provide some form of pseudo-measurement of information to update the estimates. Such patterns include zero-velocity of the foot during a normal human gait and the quantified characteristics of walking straight opposed to turning. These patterns can be captured with simple threshold algorithms or using more robust machine learning frameworks.

Another way resolve the poor performance of low-cost IMUs is to include a complementary sensor. This sensor fusion approach introduces a measurement that will correct the system's estimates by comparing the estimates with the alternative sensor's measurements. Such complementary measurements can come from cameras, ranging sensors, and other IMUs placed at different positions on the user's body. The focus of this research is to augment a dual-foot PDR system with an alternating field magnetic sensor. This novel complementary sensor will be used to correct position and attitude estimates derived from commercial-grade IMUs.

This paper focuses on the use of a new type of sensor for pedestrian navigation: an alternative magnetic field sensor that is capable of very precise location and attitude measurement with respect to the magnetic source. This sensor is combined with an IMU on each foot of the pedestrian to achieve improve navigation capabilities. By

1.3   Research Objectives

The purpose of this research it to investigate the effects of an AC electromagnetic sensor augmenting a dual-foot PDR system. Particularly, the foot position and orientation measurements from this electromagnetic sensor are used to derive foot-to-foot range and a relative rotation measurements. These measurements are fused into an IMU-based PDR system through an extended Kalman filter. This thesis intends to investigate several design choices and techniques. One technique is the use of relative

rotation measurements to correct rotational errors that may result in IMU-based applications. The other technique is the foot-to-foot range measurement. Results from using the G4 sensor as a complementary sensor to the consumer-grade IMU-based PDR system will be analyzed.

1.4   Methodology Overview

To accomplish these objectives, a IMU-based PDR system is developed. Then the accuracy of incorporating ranging measurements and relative orientations from the G4 sensor is explored. A three-phase process is followed to develop the PDR system. A dual-IMU PDR system, based on the error-state extended Kalman filter, is developed around the ADIS61470 IMU. This relatively low-cost IMU is small and lightweight enough to be mounted on the foot with negligible effect to the user's performance.

The baseline algorithm represents the first phase for the objectives. It includes only the ZUPT measurement to correct for IMU errors. The second phase builds upon the baseline by incorporating a ranging measurement. This technique has been shown to improve accuracy using foot-mounted cameras or sonar sensors [4] [5]. The third phase uses the magnetic sensor's orientation readings to calculate a relative rotation measurement to increase accuracy by correcting rotational errors.

The outputs of each phase is an estimated trajectory of the user's walk. These trajectories are generated using different combinations of measurements. All sensor data is collected during several trials. Each data-set is input into an extended Kalman filter algorithm to estimate each foot's position, velocity, and attitude. During each phase a new measurement is introduced into the Kalman filter. Each data-set is collected outdoors with a GPS module attached to the sensor setup to collect latitude, longitude, and altitude measurements of the user. These GPS readings will serve

as a ground truth to compare to the output of the pedestrian navigation system's estimated positions over time.

1.5 Document Overview

This document is organized as follows. Chapter II provides an overview of the core concepts used in this research. Chapter III details the equipment, system configuration, and technical derivations used to achieve the objective. Included is a breakdown of the sensors and how they are configured for a PDR application. This chapter also covers the design of the extended Kalman filter at the center of the system and the measurements used to optimize its output. Chapter IV presents the results of the trials conducted using the equipment and system configured in Chapter III. Finally, Chapter V discusses the overall contribution of this work and the possible next steps.

II. Background and Literature Review

A review of literature is necessary to layout a road-map of the concepts that are integral to this report's processes and results. Section 2.1 through section 2.7 will review the key concepts that form the IMU-based pedestrian navigation system. section 2.8 and section 2.9 highlights the capabilities, and limitations of IMU-based pedestrian navigation systems, and techniques to bypass these limitations.

2.1 Navigation

The purpose of navigation is to answer the fundamental questions: Where am I? Where am I going? The answers to these questions contain two pieces of information: position and velocity. Classically, ships and land-based vehicles traveled in two dimensions. As such, position measurement encompassed two axes. In the land-based case a heading measurement used to determine direction. With the development of aircraft, spacecraft, and underwater vehicles the orientation of a vehicle, aside from its position and velocity becomes important information. This attitude information represents the vehicle's orientation in 3-dimensional space. For pedestrian navigation, there is some nuance to these phenomena. Bipedal human movement, like a car on the road, travels in two dimensions. However, a dual foot, IMU-based, pedestrian navigation system will be answering those fundamental questions relative to the person's feet. As such, the foot's movement and orientation are characterized in 3-dimensional space. This culminates in a two-dimensional output of the user's position.

2.2 Dead-Reckoning

The concept of dead reckoning is thought to be derived from the phrase 'deduced reckoning' [6]. This concept involves finding a subject's position using the previous

position, the direction of travel (attitude) and the velocity. A dead reckoning system can be characterised as an internal system. These internal systems can be either passive or active [7]. Unlike systems centered around an external sensor, an internal sensor application will generate all measurements needed to determine the subject's position without any external signals. An important aspect of the dead reckoning technique is that any error incurred will be accrued to each subsequent measurement and position estimation.

2.3   Inertial Navigation Systems

A basic inertial navigation system (INS) incorporates dead reckoning with an inertial measurement unit (IMU). Many IMUs are micro-electromechanical systems (MEMS) containing gyroscopes and accelerometers for each three-dimensional axis. A gyroscope sensor measures angular rate, while the accelerometer measures specific force. The specific force represent force acting on the accelerometer, except for gravitational force. The INS system processes the data from the IMU, performing dead reckoning calculations to determine the position and attitude of the body.

2.4   Coordinate Frames

To describe the 3-dimensional position of a body a reference frame must be defined. Any position, attitude, or movement is given relative to some reference frame. A 3-dimensional coordinate frame with all axes being perpendicular to each other describes the configuration of any frame of reference in which a body is situated. That body also has 3-dimensional axes to describe it. These axes originate from a point determined for the object in question. This origin of the body's reference frame is usually set at the center the body, or the body's center of mass. These 3 axes that form the coordinate frame are usually referred to as the x, y, and z axes.

2.4.1 Navigation Frame

The Navigation Frame is aligned to a specific point of the Earth. This frame's orientation is usually aligned with geographic North, East, and Down, for x, y, and z axes respectively. Another common convention is East, North, and down for x, y, and z axes respectively.

2.4.2 Body Frame

The Body Frame is aligned to the body being tracked. Its axes align are fixed to the body. This frame is usually at the center of mass of the body. The angular motions about these axes are referred to as the roll, pitch, and yaw for the x, y, and z axes respectively.
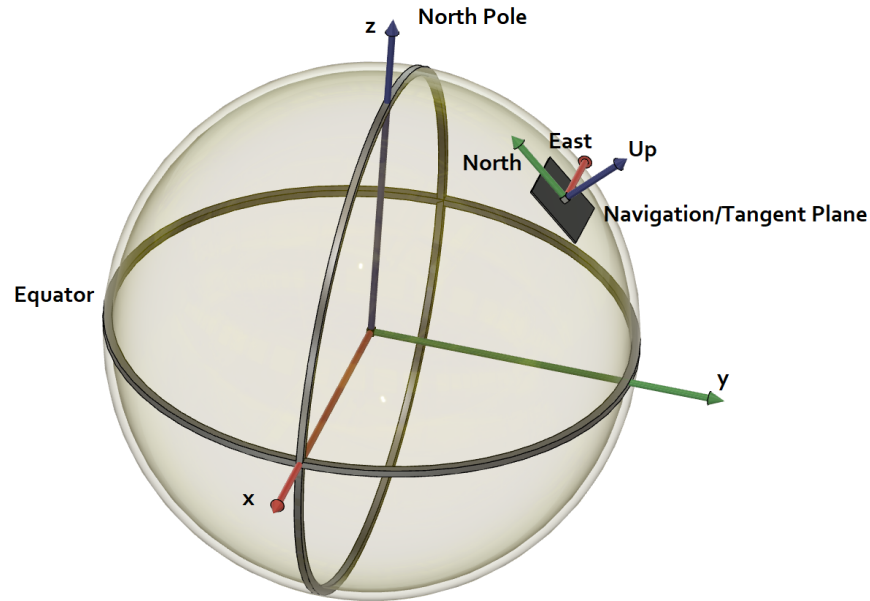
Figure 1: Globe diagram for Earth-Centered Inertial frame and Navigation frame of reference.
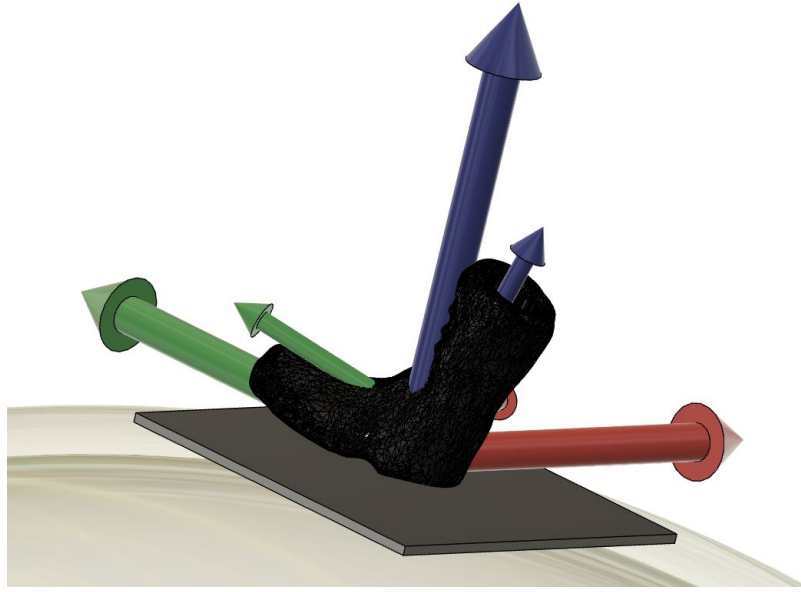
Figure 2: Diagram for Navigation and body frame of reference.

2.5   Attitude Representations

Throughout this pedestrian navigation system, the attitude of the left and right feet will be represented as Euler angles, quaternions, rotations vectors, and rotation matrices. These attitude representations are all equivalent to each other. They describe the attitude of a coordinate frame with respect to another frame. Most often this will be a body frame's orientation with respect to a navigation frame.

As summarized by P. Groves, the kinematic quantities used in this research, such as attitude and acceleration, involve three coordinate frames [6]. He denotes these frames as the object frame, α, the reference frame, β, and the resolving frame, γ. The object frame can be a body frame, while the reference frame can be a navigation frame.

2.5.1 Euler Angles

The Euler Angles represent thee successive rotations about three axes. The roll, pitch, and yaw, are the rotation about the x-axis, y-axis, and z-axis respectively. These rotations describe the orientation of the object in it's body frame with respect to the local navigation frame. Although roll, pitch, and yaw are very common terms for these rotations, other literature, such as [8], using different names. Table 1 shows some common notations of the Euler angles.

$$e = \begin{bmatrix} \psi & \theta & \phi \end{bmatrix}^T \tag{1}$$

Table 1: Euler Angle Notation

Name	Axis of Rotation	Symobl (Nav to Body)
Roll, Bank	x	ϕ_{nb}
Pitch, Elevation	y	θ_{nb}
Yaw, Azimuth, Heading	z	ψ_{nb}

2.5.2 Quaternions

The Quaternion representation is a 4-element vector representing a coordinate frame transformation about a single vector. From eq. (1), the elements of the quaternion are functions of the vector's orientation and its magnitude [6][9].

$$q = \begin{bmatrix} q_1 & q_2 & q_3 & q_4 \end{bmatrix}^T = \begin{bmatrix} w & x & y & z \end{bmatrix}^T \tag{2}$$

2.5.3 Direction Cosine Matrix

The direction cosine matrix (DCM), C_b^n, is a 3x3 matrix representation of a coordinate transformation. The columns of the DCM represent the unit vectors of the body frame with respect to a reference frame [10].

$$C_z = \begin{bmatrix} cos\psi & sin\psi & 0 \\ -sin\psi & cos\psi & 0 \\ 0 & 0 & 1 \end{bmatrix} \tag{3}$$

$$C_y = \begin{bmatrix} cos\theta & 0 & -sin\theta \\ 0 & 1 & 0 \\ sin\theta & 0 & cos\theta \end{bmatrix} \tag{4}$$

$$C_x = \begin{bmatrix} 1 & 0 & 0 \\ 0 & cos\phi & -sin\phi \\ 0 & sin\phi & cos\phi \end{bmatrix} \tag{5}$$

$$C_n^b = C_x C_y C_z \tag{6}$$

Taking the product of (3), (4), and (17) yields the DCM representation of the transformation from the navigation frame to the body frame as expressed in (18).

As Titterton, et al., [10] demonstrate, the inverse transformation from the body frame to the navigation frame require taking the transpose of the matrices in equations (3), (4), and (17).

$$C_b^n = C_z^T C_y^T C_x^T = \begin{bmatrix} cos\psi & -sin\psi & 0 \\ sin\psi & cos\psi & 0 \\ 0 & 0 & 1 \end{bmatrix} \begin{bmatrix} cos\theta & 0 & sin\theta \\ 0 & 1 & 0 \\ -sin\theta & 0 & cos\theta \end{bmatrix} \begin{bmatrix} 1 & 0 & 0 \\ 0 & cos\phi & -sin\phi \\ 0 & sin\phi & cos\phi \end{bmatrix} \tag{7}$$

$$= \begin{bmatrix} cos\theta cos\psi & -cos\phi sin\psi + sin\phi sin\theta cos\psi & sin\phi sin\psi + cos\phi sin\theta cos\psi \\ cos\theta sin\psi & cos\phi cos\psi + sin\phi sin\theta sin\psi & -sin\phi cos\psi + cos\phi sin\theta sin\psi \\ -sin\theta & sin\psi cos\phi & cos\psi cos\theta \end{bmatrix}$$

2.6   IMU Kinematics

The ADIS16470 IMUs in this research are used to estimate a pedestrian's position, velocity, and orientation. Section 2.5 discusses the representation of orientation used throughout this work. The primary quantities derived from the IMU are angular rate, position, velocity, and acceleration.

2.6.1   Angular Rate

The angular rate quantity is output from the gyroscope sensor of the IMU. The angular rate is the rate of rotation of the alpha-frame axes with respect to the beta-frame axes, resolved about the gamma-frame axes [6]. In this case, the alpha-frame represents the body-frame of the IMU, and the beta-frame represents the navigation-frame. The ADIS16470 IMU also outputs a delta-angle measurement. This measurement represents the angular displacement per sample update [11]. The angular rate is obtained from this delta-angle quantity by dividing by the sampling rate, producing a quantity in radians-per-second.

The position quantity is calculated, and estimated, at several points in this pedestrian dead reckoning approach. The position of a body refers to the placement of the body's origin of its coordinate frame with respect to the origin of a reference frame. The position vector, the red line in Figure 3, has the x, y, and z displacement components of the body-frame's origin with respect to the navigation reference frame.

The velocity quantity represents the rate of change of the position of the origin
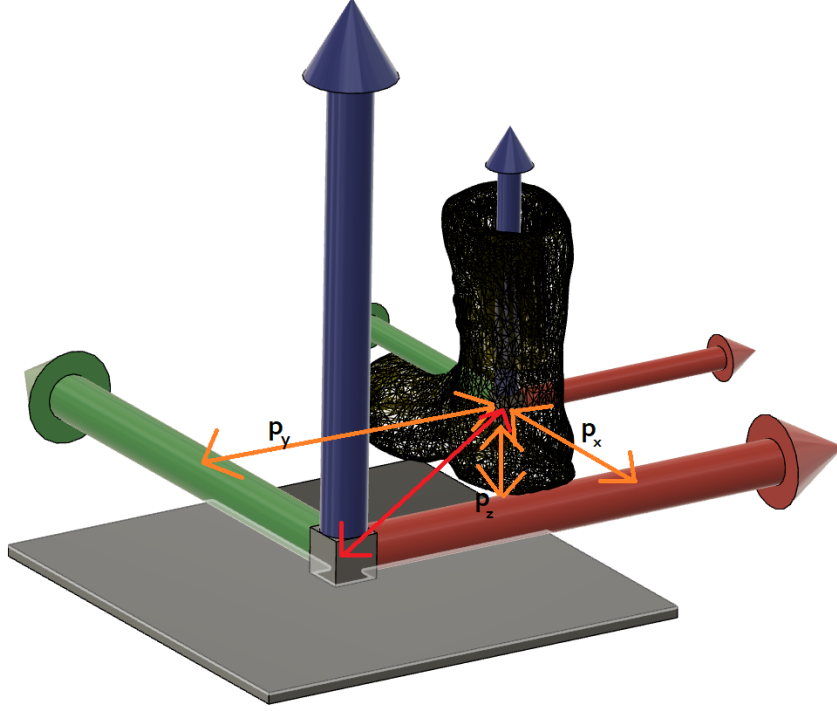
Figure 3: Diagram of body-frame (foot) position with respect to a navigation-frame. Illustrates position vector and components.

of the coordinate frame of the body with respect to the origin (position, and axes (orientation) of the reference frame [6].

The acceleration of the body represents the force per unit mass applied to the body from the perspective of the reference frame [6]. The ADIS16470 IMU outputs a delta-velocity measurement that represents the change in linear velocity per sample update [11]. This quantity is transformed to acceleration in m/s^2 by dividing by the sampling rate.

2.7 Kalman Filter

2.7.1 Linear Kalman Filter

At the heart of most pedestrian dead-reckoning systems is the Kalman Filter. The Kalman filter, Figure 4, is an estimation algorithm that can output incremental

navigation estimates such as position, velocity, and attitude. As the Kalman filter runs, measurements are fed into the filter. These measurements contain information used to correct the Kalman filter's estimates. The construction of the Kalman filter is based on the dynamics of the system being estimated. Both the Kalman filter's process and the measurements fed into it have addative white Gaussian noise associated with them.

A Kalman filter is constructed based on the configurations of the system model and its inputs to produce as accurate a set of estimates as the system's given information can produce [6]. From one step to the next, the Kalman filter keeps track of how uncertain its estimates are, along with the correlations between the error in the estimates and its parameters. With each iteration the Kalman Filter updates it's estimates stemming from initial estimates. Each estimate is optimized as a weighted average of the past set of estimates, and the current estimates based on the usefulness of the current iteration's measurements and the measurement's error statistics [12].

Initial State   Prediction/Propagate

$$\hat{\mathbf{x}}_k^- = A\hat{x}_{k-1} + Bu_{k-1}$$
$$P_k^- = AP_{k-1}A^\top + Q$$

$\mathbf{x}_0$

P_0

$k \leftarrow k+1$

Measurement Update/ Innovation

$$K_k = P_k^- H^\top (HP_k^- H^\top + R)^{-1}$$
$$\hat{\mathbf{x}}_k = \hat{\mathbf{x}}_k^- + K_k \left(z_k - H\hat{\mathbf{x}}_k^-\right)$$
$$P_k = (I - K_k H)P_k^-$$
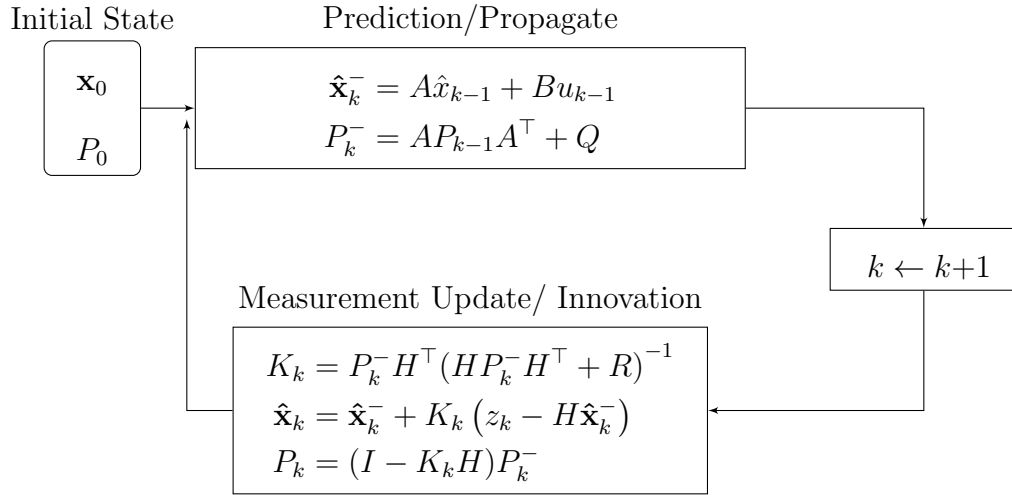
Figure 4: Discrete Kalman Filter Algorithm

A linear system's dynamics can be modeled with the set of first order differential equations (8) [10][13]. The system's associated measurements (9) can also be modeled with the same conventions.

Table 2: Linear system Dynamics

Name	Description
x	states of the system
u	deterministic input vector
w	system noise
z	measurement vector
n	measurement noise
A	system matrix
B	system input matrix
Q	process noise covariance matrix
R	measurement noise covariance matrix
H	measurement matrix

$$x_k = Ax_{k-1} + Bu_k + w_{k-1} \tag{8}$$

$$z_k = Hx_k + v_k \tag{9}$$

The process noise, w, and the measurement noise, v, are zero-mean, normally distributed Gaussian vectors, with probability distributions of $\mathcal{N}(0, Q)$ and $\mathcal{N}(0, R)$ respectively.

2.7.2 Extended Kalman Filter

An important assumption for the Kalman filter is that both the measurement model and system model are linear systems. This linearity cannot be assumed for real systems, particularly INS systems. The Extended Kalman Filter (EKF) is a nonlinear extension of standard Kalman Filter. To account for the non-linearity, the estimates are linearized around the current estimate by using the partial derivatives of the state and measurement functions [14].

$$x_k = f(x_{k-1}, u_k, 0) \tag{10}$$

$$z_k = h(x_k, 0) \tag{11}$$

The system's equations are linearized about (12) and (13). For real systems the exact value of the process noise, w_k, and the measurement noise, v_k, are not known. The state and measurement vectors can still be approximated without them [14].

$$x_k \approx \widetilde{x}_k + A(x_{k-1} - \hat{x}_{k-1}) + W_{w_{k-1}} \tag{12}$$

$$z_k =\approx \widetilde{z}_k + H(x_k - \widetilde{x}_k) + V_{v_k} \tag{13}$$

Initial State   Prediction/Propagate

$\mathbf{x}_0$

P_0

$$\hat{\mathbf{x}}_k^- = f(x_{k-1}, u_k, 0)$$
$$P_k^- = AP_{k-1}A^\top + WQ_{k-1}W^\top$$

$$k \leftarrow k+1$$

Measurement Update/ Innovation

$$K_k = P_k^- H^\top (HP_k^- H^\top + VR_kV^\top)^{-1}$$
$$\hat{\mathbf{x}}_k = \hat{\mathbf{x}}_k^- + K_k \left(z_k - h(\hat{x}_k^-, 0) \right)$$
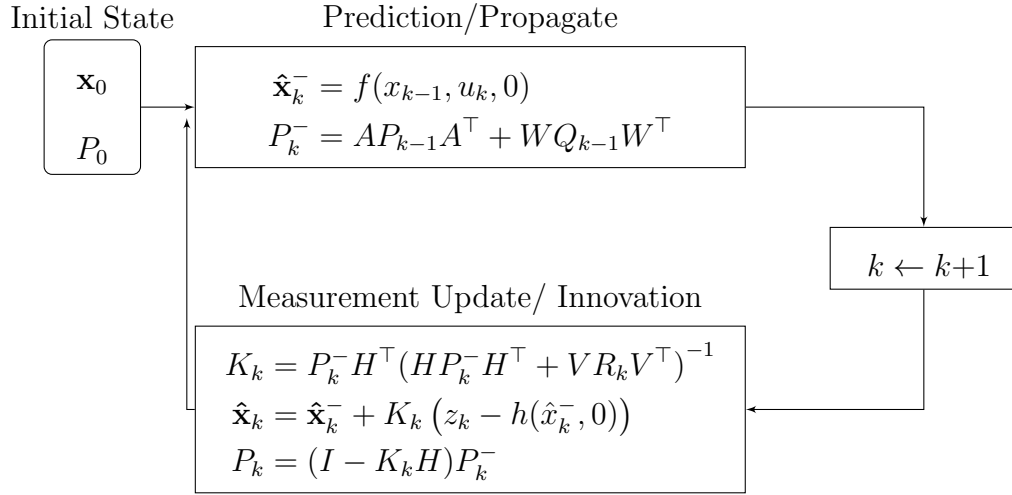$$P_k = (I - K_kH)P_k^-$$

Figure 5: Extended Kalman Filter Algorithm

Note that the Jacobian matrices A, W, H, and V also change with each step, k.

Table 3: Non-Linear system Dynamics

Name	Description
x_k	state vector
z	measurement vector
$\widetilde{x}_k$	approximated state vector
$\widetilde{z}_k$	approximated measurement vector
k	previous state estimate
w	process noise
v	measurement noise
A	Jacobian matrix of partial derivatives of f with respect to x
H	Jacobian matrix of partial derivatives of h with respect to x
W	Additive White Gaussian Noise
V	Additive White Gaussian Noise

2.8 Zero Velocity Update

As the issues associated with pedestrian navigation are essentially the same issues associated with dead reckoning, several techniques have been previously introduced to help mitigate the effects of these errors. For pedestrian navigation, a specific group of techniques have been introduced that utilize unique characteristics of the human gait pattern to optimize these PDR systems. These techniques include the Zero Velocity Update (ZUPT), the Zero Angular Rate Update (ZARU), and the Heuristic Drift Reduction (HDR) [15][16]. The ZUPT technique uses a pseudo-measurement of a zero velocity vector as a measurement into a Kalman filter to fix drift errors in the IMU. This technique uses the assumption that a normal human gait pattern involves a velocity of approximately zero during the stance phase of a stride [17]. Similarly, the ZARU technique uses a pseudo-measurement of zero angular rate vector [18]. The measurement is also detected and input into the Kalman filter during the same stance phase as ZUPT. The HDR technique determines when a pedestrian is walking a straight line and applies a heading error measurement into the Kalman filter to reduce heading estimate errors. [16].

2.9   Related Research

The purpose of a Pedestrian Navigation System (PNS) is to provide accurate means of position tracking in GPS deprived environments. An important aspect of these systems are the use of sensors to capture pedestrian motion. Two primary means of capturing this motion involve vision-based sensors [19] and IMUs attached to the pedestrian's body [20][21][17]. There are some cases where both sensor types paired together to acheive the PNS purpose [4]. These sensors act as the input source for the Kalman filter at the heart of the PNS implementation.

2.9.1   Vision-Based PDR

In the robotics and navigation fields, the problem of localization is essential for creating a robust system. Whether a robot, a vehicle, or a person, the knowledge of that subject's position and orientation [?]. Depending on the circumstances of the system, the subject's pose information can be relative to the world or local to a specific boundary such as a certain room withing a building. For vision-based localization systems the optical sensor can be such things as a camera. This sensor being fixed to the subject, has its pose computed with reference to its surrounding environment. Simultaneous Localization And Mapping (SLAM) systems compute the vision sensor's pose by detecting environment features, matching them with previously detected features in past images, to build a map of the subject's area and the subject's pose within it [19]. These vision-based solutions require ideal environment conditions, for the optical sensors to provide useful information. They also use substantial computing power.

2.9.2 IMU-Based PDR Systems

Fischer, et al., have introduced a tutorial for basic IMU-based, pedestrian dead reckoning system [21]. Their implementation forms the basis of the PDR system used in this research. Key features used from their tutorial include the ZUPT detection algorithm, usage of an error-state EKF, and handling orientation extrapolations as rotation matrices. The work of Jimenez, et al., extends the PDR system further by incorporating ZARU, and HDR techniques along with the ZUPT technique to achieve improved system accuracy [15]. Foot-to-foot range measurement were introduced as a valid measurement to reduce IMU associated errors in the PDR system [5]. While many of these PDR contributions were achieved with a single foot's motion being captured, the range measurement requires IMUs on both feet. With two IMUs it is necessary to extend the Kalman filter's state vector with pose states for the left and right foot. The dual PDR system also requires the usage of two ZUPT algorithms, one for each foot. The camera and sonar sensor are two of the sensors that have been shown to provide measurements that can calculate foot-to-foot range [5] [4].

III. Methodology

Preamble

This chapter, will provide descriptions of the tools, structure, and parameters used to carry out this research. Included will be description of the core measurements ,the sensors that provide them, and the derivations of the their data to optimize the Pedestrian Dead Reckoning (PDR) system. Portions of this section are sourced from the following paper [22].

3.1   Development Framework

The objectives of this research were to introduce a novel device, the Polhemus G4 sensor system, into the PDR field, use the G4 sensor's position measurement to incorporate ranging measurements into the PDR system, and introduce a new measurement configuration called relative rotation measurement update. The accomplish these objectives a three phase strategy was used.

1. Phase 1: Sensor Configuration and Data Collection

   - Capture IMU, G4 sensor, and GPS data

2. Phase 2: Build PDR System

   - Single-Foot PDR system

   - IMU Mechanization

   - Implement ZUPT Algorithm

   - Dual-Foot PDR system

3. Phase 3: Incorporate Polhemus G4 Sensor System

- Foot-to-Foot Range measurement

- Relative Rotation Measurement

3.2 Phase 1: Sensor Configuration and Data Collection

The sensors primarily used in this PDR system are two Analog Devices ADIS16470 IMUs Figure 6 and one Polhmeus G4 sensor kit shown in Figure 8. For each foot, an IMU and a magnetic sensor is strapped to the user's foot via a 3D printed case. The case encloses the IMU with the magnetic sensor on top of the lid of the case, directly above the ADIS16470 IMU. The case has a strap used to attach the sensors to a boot used in the trials (see Figure 7). The cables from the foot-mounted sensors run up the user's leg directly to the PC, IMUs, or to the G4 transmitter.
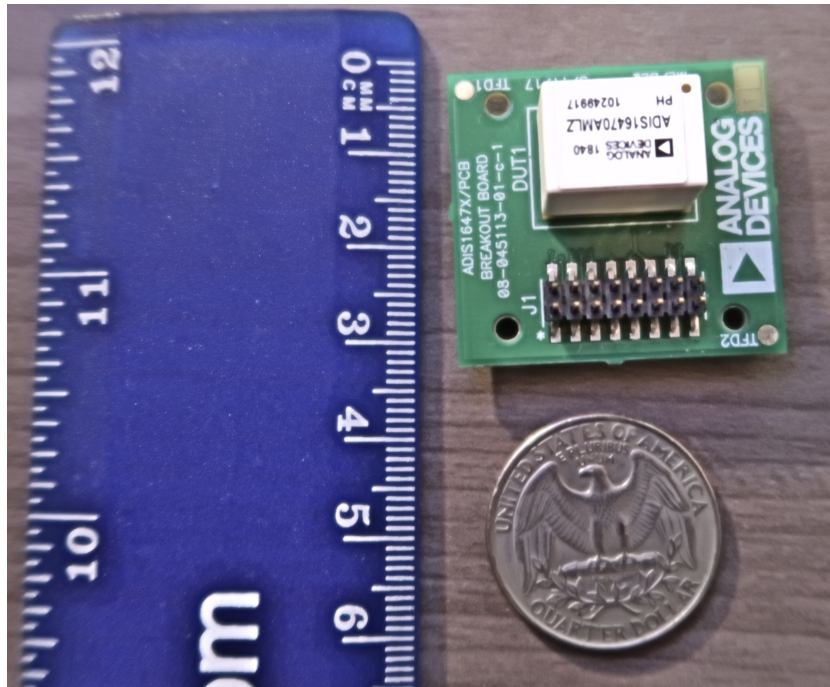
Figure 6: ADIS16470 IMU

The ADIS16470 sensors output delta-velocity and delta-theta values at 100 Hz. An Arduino Nano interfaces with the IMU. A Linux-based PC then interfaces to

the Arduino with a set of custom drivers based on Lightweight Communications and Marshalling (LCM).

Figure 7: IMU and G4 sensor strapped to boot

In addition to the magnetic sensor itself, the magnetic sensors also require a "source" and a data transmitter/receiver pair [8]. The model used in this research is a Polhemus G4 where the source is a small cube (mounted on the backpack in Figure 9), the receiver is a USB dongle that passes the data onto a computer and the transmitter is a small belt-mounted device that wirelessly communicates with the receiver while feeding power to and getting data from the sensors through wired connections (Figure 8).

The G4 system outputs position measurements relative to the source in Cartesian, coordinates and sensor attitude measurements expressed as the Euler angles azimuth, elevation, and roll. The origin of reference frame, of which each magnetic sensor's measurements are relative to, is the position of the source. The G4 system's source produces a magnetic field which the magnetic sensors are sensed within. The source's position is fixed to the user, as shown in fig. 9. The G4 system also includes a wireless tracking unit, called the "hub", that can connect up to three magnetic sensors, and

Figure 8: Polhemus G4 Sensor, transmitter, and receiver

a USB module that pairs the hub to a host PC to transmit the measurements of the magnetic sensors wirelessly.

The accuracy of the the magnetic sensor's measurements are relative to the sensor's distance from the source. Each transmitter is capable of providing measurement for up to three sensors simultaneously [8]. The source emits an electromagnetic field, which is used to track the position and orientation of the small sensors. The output of the magnetic sensors is a 100 Hz 3d position and orientation, relative to the magnetic source.

To complete the system setup, the rig backpack also has a battery pack to power the magnetic source and a GPS unit. The GPS unit is not used by the system to estimates the user's position, it is only used to provide truth data. As with the IMUs, the G4 sesnors and GPS measurements are all read with custom drivers using the LCM framework through a Linux-based PC.
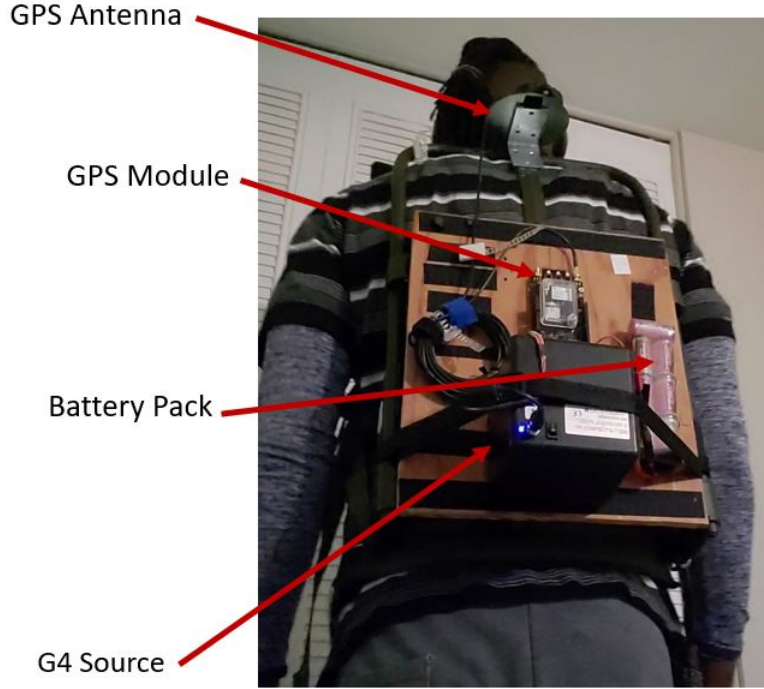
Figure 9: G4 source, battery pack, and GPS module and antenna on backpack rig

3.3 Phase 2: PDR System

Phase 2 of the methodology consists of building out the Kalman filter. This phase started out with a single foot estimation then later expanded to dual foot system, as shown in fig. 10. All system parameter expressed from here will have dimensions that reflect the dual-foot implementation.

To perform pedestrian dead reckoning, an extended Kalman filter (EKF) estimation routine is utilized. At the core of algorithm is the mechanization of each IMU to propagate position and attitude to the current IMU measurement. This mechanization is discussed in the first subsection below, followed by the (error state) Kalman filter implementation of that mechanization. The last 3 subsections describe different measurements that are applied to improve the IMU-based mechanization: the zero velocity update (ZUPT), and relative ranging estimate, and a relative rotation measurement.
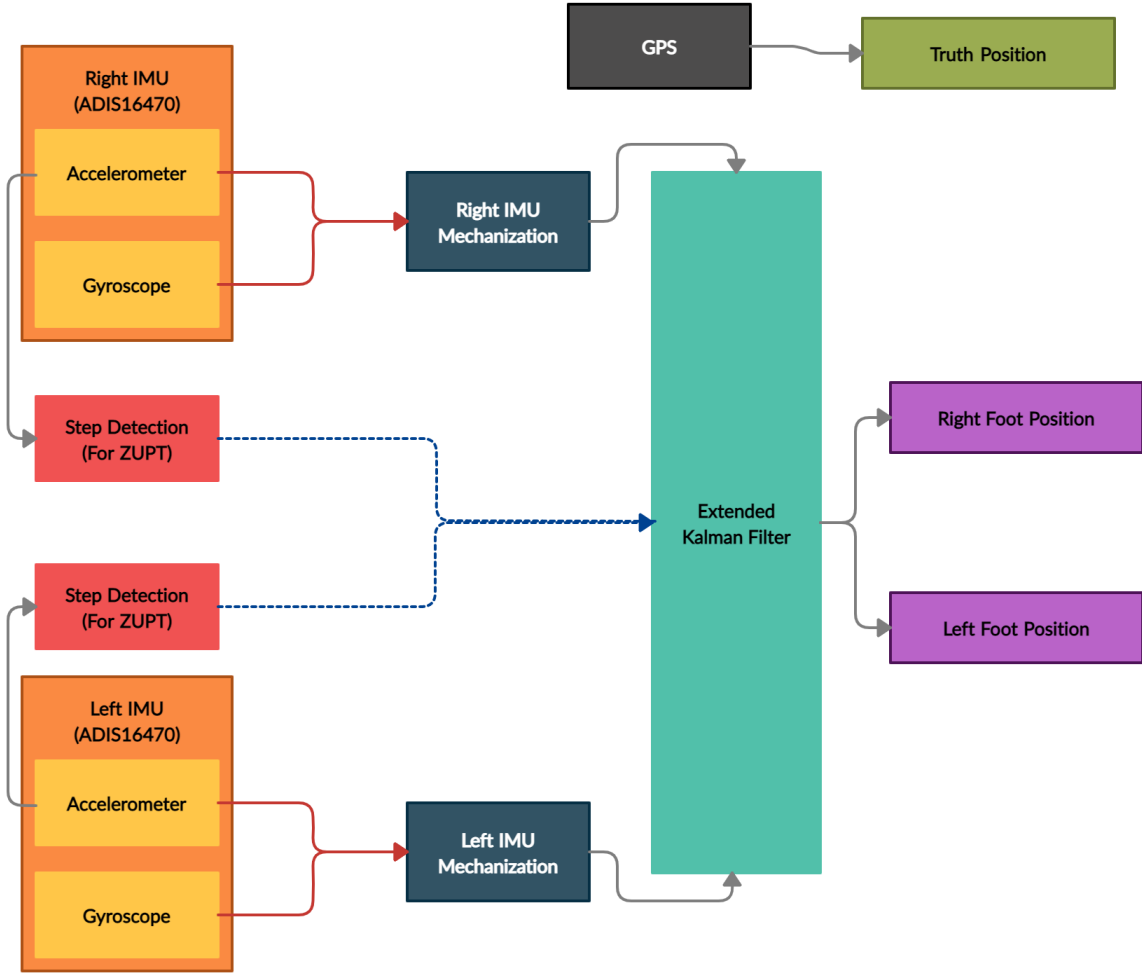
Figure 10: PDR System Configuration

3.3.1   IMU Mechanization

This algorithm uses an error-state extended Kalman filter to account for orientation, position, and velocity errors. The error-state vectors representation is as follows:

$$
\delta_x = \begin{bmatrix} \delta_{\phi_r} \\ \delta_{\omega_{b_r}} \\ \delta_{p_r} \\ \delta_{v_r} \\ \delta_{b_r} \\ \delta_{\phi_l} \\ \delta_{\omega_{b_l}} \\ \delta_{p_l} \\ \delta_{v_l} \\ \delta_{b_l} \end{bmatrix}_{30 \times 1}
\tag{14}
$$

The subscripts l and r representing the state associated with the left or right foot respectively. The states δ_ϕ, δ_p, and δ_v, represent attitude, or orientation, position, and velocity error, respectively. The states $\delta_{\omega_{b_r}}$ and δ_{b_r} are the gyroscope bias and accelerometer bias estimates respectively. Each state has three axis components, x, y, z, forming a 30 element state vector.

The accelerometer and gyroscope initial biases are calculated as the mean of the initial 2000 samples. This occurs before the recorded data is filtered through the Kalman filter. These samples represent the the initial stationary data recorded from the IMUs in which the user remains still. The bias calculations are subtracted from the gyroscope and accelerometer readings. Each foot's orientation is then calculated using the bias compensated angular rate readings within a skew symmetric matrix shown in eq. (15).

$$
\Omega_k = \begin{bmatrix} 0 & -\omega_z & \omega_y \\ \omega_z & 0 & -\omega_x \\ -\omega_y & \omega_x & 0 \end{bmatrix}_{3 \times 3}
\tag{15}
$$

This orientation calculation, eq. (16), represents an integration of the angular rate data. To abate the difficulties of calculating the matrix exponential in orientation calculation, the Padé approximation is used [23] [24].

$$C_{IMU_k}^{Nav} = C_{IMU_{k-1}}^{Nav} exp(\Omega_k \Delta t) = C_{IMU_k}^{Nav} \frac{2I_{3\times3} + \Omega_k \Delta t}{2I_{3\times3} - \Omega_k \Delta t} \tag{16}$$

$$= C_{IMU_k}^{Nav}(2I_{3\times3} + \Omega_k \Delta t)(2I_{3\times3} - \Omega_k \Delta t)^{-1}$$

where C_{IMU}^{Nav} is the rotation matrix of either the left or right foot's IMU from the IMU's body frame to the navigation frame, post-multiplied by the matrix exponential term since the matrix exponential term is with respect to the IMU's frame of reference.

The acceleration data is transformed to the navigation frame then the gravity components are subtracted from the accelerometer readings. As Fischer, et al. proposed, the average of the previous and the current orientation calculations are taken to account for the motion between measurements [21].

$$acc_k^{Nav} = \frac{1}{2}(C_{IMUk}^{Nav} + C_{IMUk-1}^{Nav})(acc_k^{IMU}) \tag{17}$$

After this transformation, the gravity term is subtracted from the acceleration data within the integration calculation that yields the velocity estimate. The constant sampling rate, with relatively small range, allows the use of the trapezoidal integration scheme to obtain the velocity [10].

$$vel_k = vel_{k-1} + \frac{(acc_k - g) + (acc_{k-1} - g)}{2}dt \tag{18}$$

Now the velocity estimate is integrated in the same manner to obtain the position estimate.

$$pos_k = pos_{k-1} + \frac{vel_k + vel_{k-1}}{2}dt \tag{19}$$

3.3.2 Error State Extended Kalman Filter

While the position estimate for each IMU is propagated as described in section 3.3.1, an error-state Kalman filter is used to find the errors of that propagation, as described in [5][15]. When using an error state EKF, essentially two state vectors are propagated forward. The first state, known as the *nominal state*, is the full estimate (position, velocity, attitude, sensor biases) based on each IMU. The nominal states are extrapolated from the IMU mechanization equations from section 3.3.1. The second state, the error state eq. (14), is calculated by the Kalman filter's measurement updates. This error state represents the improvements, or updates, for the nominal states. During every time step, once calculated, the error states are subtracted from the nominal states to improve the nominal estimates, then the error states are set back to 0. This reset occurs because the nominal states already account for the past errors.

The errors of the propagation are modeled using a linearized state model defined as:

$$\delta X_k = \Phi \delta X_{k-1} + W_{k-1} \tag{20}$$

Where Φ is the state transition matrix of the form:

$$\Phi_{k_{r,l}} = \begin{bmatrix} I_{3\times3} & \Delta t \cdot C_{IMU_{k-1}}^{Nav} & 0_{3\times3} & 0_{3\times3} & 0_{3\times3} \\ 0_{3\times3} & I_{3\times3} & 0_{3\times3} & 0_{3\times3} & 0_{3\times3} \\ 0_{3\times3} & 0_{3\times3} & I_{3\times3} & \Delta t \cdot I_{3\times3} & 0_{3\times3} \\ -\Delta t \cdot S_k & 0_{3\times3} & 0_{3\times3} & I_{3\times3} & \Delta t \cdot C_{IMU_{k-1}}^{Nav} \\ 0_{3\times3} & 0_{3\times3} & 0_{3\times3} & 0_{3\times3} & I_{3\times3} \end{bmatrix}_{15\times15} \tag{21}$$

$$\Phi_k = \begin{bmatrix} \Phi_{k_r} & 0_{15\times15} \\ 0_{15\times15} & \Phi_{k_l} \end{bmatrix}_{30\times30} \tag{22}$$

The S_k term, eq. (23), used in eq. (21) represents the skew symmetric matrix of the bias corrected accelerometer terms in the navigation frame. The S_k matrix allows the EKF to estimate the pitch and roll based on accelerometer values [15]

$$S_k = \begin{bmatrix} 0 & -acc_{k_z}^{Nav} & acc_{k_y}^{Nav} \\ acc_{k_z}^{Nav} & 0 & -acc_{k_x}^{Nav} \\ -acc_{k_y}^{Nav} & acc_{k_x}^{Nav} & 0 \end{bmatrix}_{3\times3} \tag{23}$$

In the state model, W_{k-1}, eq. (24) and eq. (25), is the process noise with the covariance matrix defined with the following diagonal elements:

$$Q_{k_{r,l}} = diag\left(\begin{bmatrix} \sigma_\omega & \sigma_{g_b} & \sigma_p & \sigma_v & \sigma_{a_b} \end{bmatrix}\right)_{15\times15} \tag{24}$$

$$Q_k = \begin{bmatrix} Q_{k_r} & 0_{9x9} \\ 0_{9x9} & Q_{k_l} \end{bmatrix}_{30\times30} \tag{25}$$

These elements are listed in table 4. The error covariance matrix for each step is then propagated forward.

29

Table 4: Process Noise Parameters

Parameter	Notation	Value
Attitude	σ_ω	0.016 rad/s
Velocity	σ_v	0.030 m/s
Position	σ_p	0.000 m
Gyroscope Bias	σ_{g_b}	0.002 rad/s
Accelerometer Bias	σ_{a_b}	0.000 m/s^2

$$P = \Phi_k P_{k-1} \Phi_k^T + Q_k \tag{26}$$

The state update equation takes the form:

$$\delta_{X_k} = \delta_{X_{k-1}} + K_k(m_k - H\delta_{x_{k-1}}) \tag{27}$$

To update position and velocity components of the nominal states, their corresponding error-state vector portions are directly subtracted from their values.

$$pos_k^+ = pos_k^- - pos_{\epsilon,k} \tag{28}$$

$$vel_k^+ = vel_k^- - vel_{\epsilon,k} \tag{29}$$

Where the $-$ and $+$ superscripts represent the nominal state before and after correction by the error states, respectively. Once all nominal states have been corrected, the error-state estimates are set to zero.

For the orientation, a skew-symmetric correction matrix of the orientation error estimations is applied to the previous orientation matrix. The last updated orientation matrix is pre-multiplied by this correction calculation, as the correction matrix is with respect to the navigation frame. The aforementioned Padé approximation is

used here:

$$C_{IMU_k}^{Nav+} = \frac{2I_{3x3} + \Omega_{\epsilon,k}}{2I_{3x3} - \Omega_{\epsilon,k}} C_{IMU_k}^{Nav-} = (2I_{3\times3} + \Omega_{\epsilon,k})(2I_{3\times3} - \Omega_{\epsilon,k})^{-1} C_{IMU_k}^{Nav-} \qquad (30)$$

$$\Omega_{\epsilon,k} = \begin{bmatrix} 0 & \omega_{\epsilon_z,k}^{Nav} & -\omega_{\epsilon_y,k}^{Nav} \\ -\omega_{\epsilon_z,k}^{Nav} & 0 & \omega_{\epsilon_x,k}^{Nav} \\ \omega_{\epsilon_y,k}^{Nav} & -\omega_{\epsilon_x,k}^{Nav} & 0 \end{bmatrix}_{3x3} \qquad (31)$$

3.3.3   Zero Velocity Update (ZUPT)

The first measurement update applied in our system is the commonly used ZUPT update based on the still phase of human gait [5][4][25][15]. When walking, humans always have one of their two feet "planted" on the ground while their other foot moves. For example, in Fig.11, during the movement forward of the left foot, the right foot is planted to the ground. When a foot is planted, it has a velocity of approximately zero. A zero velocity state is detected when the foot acceleration falls within a simple threshold, and when the angular velocity falls within a threshold. Once detected, a "pseudo-measurement" of zero velocity is applied using a Kalman filter update.

The ZUPT update measurement matrix, H, is a 3 by 18 matrix with an identity matrix representing error-state velocity for the right or left ZUPT detection:

$$H_r = \begin{bmatrix} 0_{3\times3} & 0_{3\times3} & 0_{3\times3} & I_{3\times3} & 0_{3\times3} & 0_{3\times3} & 0_{3\times3} & 0_{3\times3} & 0_{3\times3} & 0_{3\times3} \end{bmatrix}_{3\times30} \qquad (32)$$

$$H_l = \begin{bmatrix} 0_{3\times3} & 0_{3\times3} & 0_{3\times3} & 0_{3\times3} & 0_{3\times3} & 0_{3\times3} & 0_{3\times3} & 0_{3\times3} & I_{3\times3} & 0_{3\times3} \end{bmatrix}_{3\times30} \qquad (33)$$

31

Figure 11: Walking, foot with zero velocity

Here the error measurement, m_k, for the ZUPT update, consists of the difference between the *nominal* velocity and the 0-vector pseudo-measurement:

$$m_k = v_{k-1} - [0, 0, 0] \tag{34}$$

With each measurement update, the error-state vector corrects the nominal state then is set to zero. As such, for the new measurement calculating the error-state vector equation simplifies to:

$$\delta_{x_k} = \delta_{x_k}^- + K_k(m_k - H\delta_{x_k}^-) = K_k(m_k) \tag{35}$$

where $\delta_{x_k}^-$ is the error state before the update, K is the Kalman gain,

$$K_k = P_k H^T (H P_k H^T + R)^{-1} \tag{36}$$

and R is the covariance matrix of the pseudo-measurement, a value determined by

gain tuning with data from the system.

3.4 Phase 3: G4 Sensor Measurements

This phase contains the primary contributions of this work to the field of PNS and PDR systems. The G4 sensor's drift-free measurements are incorporated into the PDR system, Figure 12. Because each time step of this filter is equal to the sensor rate, 1/100 second, the position and orientation measurements are used to correct the nominal states at every step, k. This is unlike the ZUPT pseudo-measurements which are used only when a zero-velocity is detected.

3.4.1 Foot-to-foot Ranging

Another measurement used to refine the two IMU's mechanization approximations is the range between the two IMUs. For the foot-to-foot range measurement the nominal state's x, y, z position differences are used to calculate the overall range (magnitude) of the difference between the IMUs. The same differences and magnitude is calculated for the magnetic sensors. In Figure 13 the distance between the left foot and right foot, based on either the IMU-based position estimates or the position measurements from the G4 sensors, is illustrated.

To update the error state requires both the computation of the *predicted* range, from the nominal and error states, and the *measured* range from the magnetic sensors. The range will be constant across coordinate frames, so the IMU equations are:

$$diff_x^{IMU} = pos_{k_{x_r}} - pos_{k_{x_l}} \tag{37}$$

$$diff_y^{IMU} = pos_{k_{y_r}} - pos_{k_{y_l}} \tag{38}$$

$$diff_z^{IMU} = pos_{k_{z_r}} - pos_{k_{z_l}} \tag{39}$$
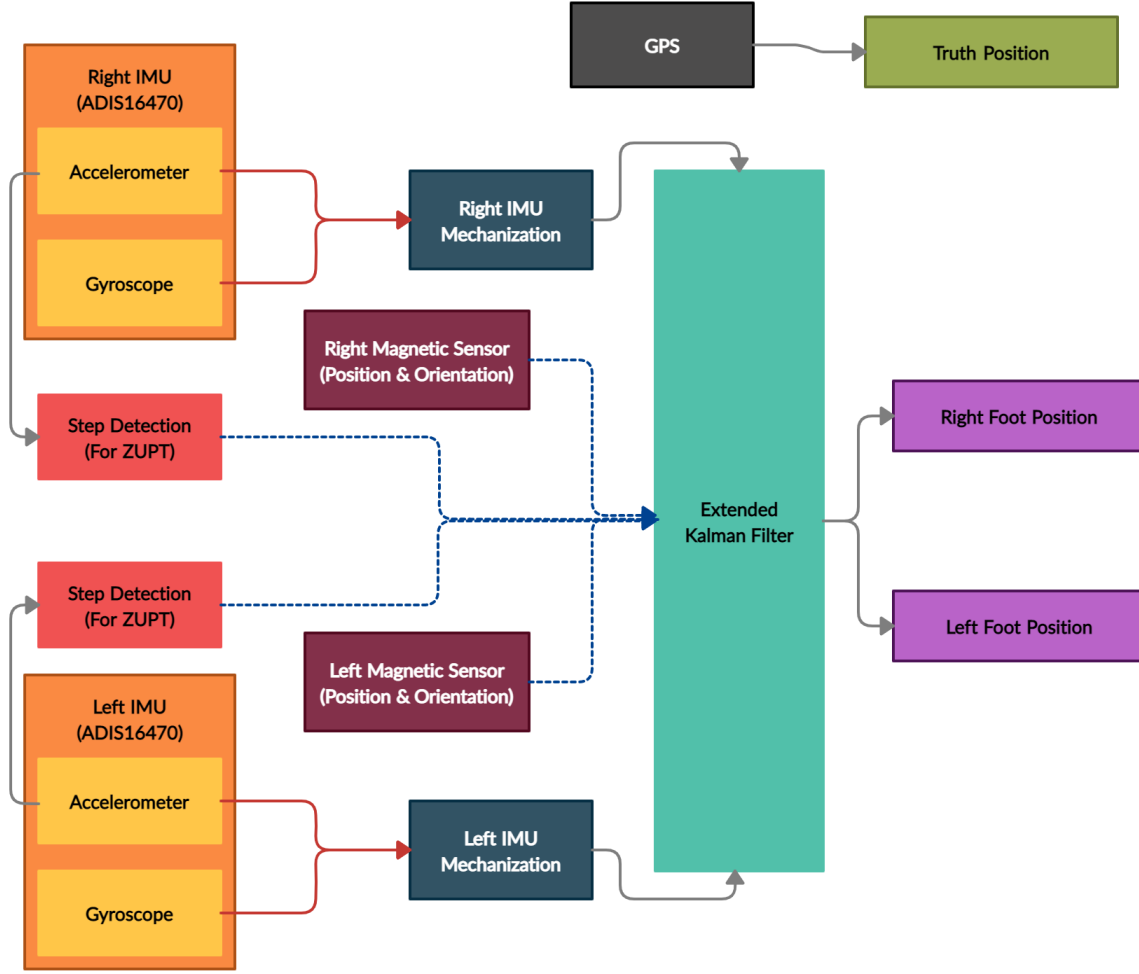
Figure 12: PDR System with Magnetic Measurements

$$mag^{IMU} = \sqrt{(diff_x^{IMU})^2 + (diff_y^{IMU})^2 + (diff_z^{IMU})^2} \tag{40}$$

where the $pos_\square$ terms are computed as shown in Equation (28) (but without necessarily resetting the error states to 0.)

Similarly, for the range between magnetic sensors:

$$diff_x^{Magnetic} = pos_{k_{x_r}}^{Magnetic} - pos_{k_{x_l}}^{Magnetic} \tag{41}$$

$$diff_y^{Magnetic} = pos_{k_{y_r}}^{Magnetic} - pos_{k_{y_l}}^{Magnetic} \tag{42}$$

Figure 13: Walking, foot-to-foot ranging measurement

$$diff_z^{Magnetic} = pos_{k_{z_r}}^{Magnetic} - pos_{k_{z_l}}^{Magnetic} \tag{43}$$

$$mag^{Magnetic} = \sqrt{(diff_x^{Magnetic})^2 + (diff_y^{Magnetic})^2 + (diff_z^{Magnetic})^2} \tag{44}$$

The left and right measurement matrices are then formed using the calculations from equations 37-44.

$$H_{right} = \frac{1}{mag^{IMU}} \begin{bmatrix} 0_{1\times6} & diff_x^{IMU} & diff_y^{IMU} & diff_z^{IMU} & 0_{1\times6} \end{bmatrix}_{1\times15} \tag{45}$$

$$H_{left} = \frac{1}{mag^{IMU}} \begin{bmatrix} 0_{1\times6} & -diff_x^{IMU} & -diff_y^{IMU} & -diff_z^{IMU} & 0_{1\times6} \end{bmatrix}_{1\times15} \tag{46}$$

$$H_{range} = \begin{bmatrix} H_{right} & H_{left} \end{bmatrix}_{1 \times 30} \tag{47}$$

The error measurement for the foot-to-foot range is formed as:

$$m = mag^{IMU} - mag^{Magnetic} \tag{48}$$

which is multiplied by a K matrix to update the mean and covariance of the error states.

3.4.2 Relative Rotation Measurement

The most novel measurement included in our system is the relative rotation between the IMUs. The idea, illustrated in Fig.14, is to take the rotation from one foot to the other, based on the IMUs, and compare it to the rotation from the same foot to the other based on the magnetic sensors' attitude measurements.
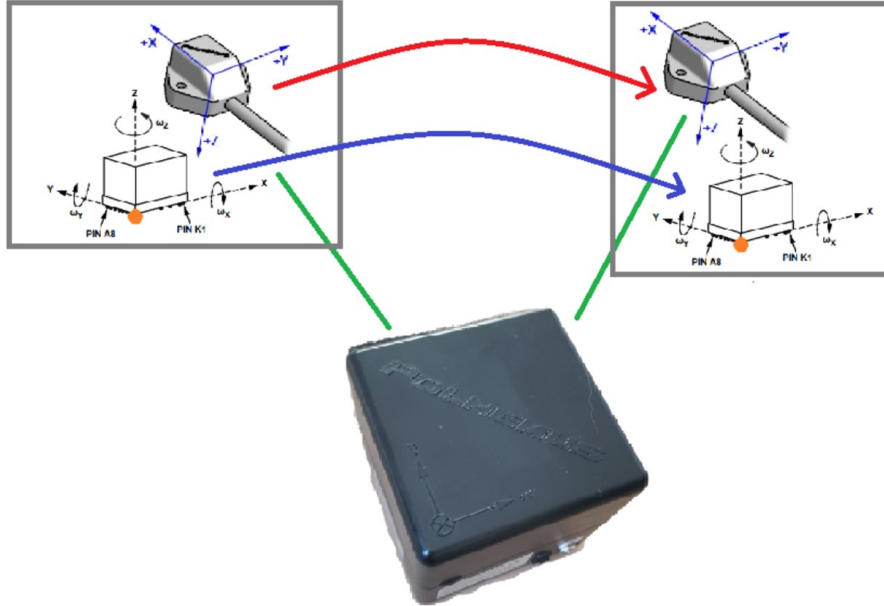
Figure 14: Relative Rotation Diagram

As shown in Figure 14, there are several different coordinates frames that must

be understood to perform the Kalman filter update using relative rotation. First, the measurements of the magnetic sensors are given with respect to (w.r.t.) the magnetic source. Therefore, there are actually two measurements, denoted as $C_{Source}^{Mag_r}$ and $C_{Source}^{Mag_l}$ for the right and left magnetic sensor, respectively. These are combined into a single relative rotation matrix as:

$$C_{Mag_l}^{Mag_r} = C_{Source}^{Mag_r} \left(C_{Source}^{Mag_l} \right)^\top \tag{49}$$

Second, to generate a predicted measurement, the relative rotation between IMUs is computed as:

$$C_{IMU_l}^{IMU_r} = C_{Nav}^{IMU_r} \left(C_{Nav}^{IMU_l} \right)^\top \tag{50}$$

Note, however, that the IMU and Mag coordinate frames are not aligned with each other based on how the sensors are mounted. To account for this, the rotations to the Mag frame from the IMU frames must be added by using rotations from IMU to Magnetic sensor coordinate frames eq. (51).

$$C_{Mag}^{IMU} = \begin{bmatrix} 0 & 1 & 0 \\ 1 & 0 & 0 \\ 0 & 0 & -1 \end{bmatrix}_{3\times3} \tag{51}$$

To perform the actual measurement update, we express the relative rotation as a 3-element vector. To obtain this vector, the rotation matrix is expressed as a matrix exponential of a skew symmetric matrix (S). These relationships are expressed as:

$$C_{IMU_l}^{Nav} = expm(S_{IMU_l}) \tag{52}$$

$$S_{IMU_l} = logm(C_{IMU_l}^{Nav}) \tag{53}$$

where *expm* and *logm* are the matrix exponential and logarithm, respectively. Furthermore, the skew-symmetric matrix can be transformed to a 3-vector (symbolized by $SS2v(S)$) and back to a skew-symmetric matrix (represented as $[v]_\times$), with the following relations:

$$S = [v]_\times = \begin{bmatrix} 0 & v_3 & -v_2 \\ -v_3 & 0 & v_1 \\ v_2 & -v_1 & 0 \end{bmatrix}_{3\times3} \tag{54}$$

$$SS2v(S) = \begin{bmatrix} v_1 & v_2 & v_3 \end{bmatrix} \tag{55}$$

Using these relationships, the complete measurement from the magnetic sensors is expressed as:

$$SS2v\left(logm\left(C_{Source}^{Mag_r}\left(C_{Source}^{Mag_l}\right)^\top\right)\right) \tag{56}$$

The predicted measurement, using the rotations from IMU to a common nav frame as defined in Equation (30) is:

$$z = SS2v\left(logm\left(C_{IMU_r}^{Mag_r}C_{Nav}^{IMU_r}\left(C_{IMU_l}^{Mag_l}C_{Nav}^{IMU_l}\right)^\top\right)\right) \tag{57}$$

where z is a 3-vector representing the full predicted measurement.

This leads to both a measurement and predicted measurement that is a 3-vector. To find the derivative of the predicted measurement w.r.t. the error states, we use the derivative of the $SS2v(logm(C))$ function as derived in [26]. Note that C is assumed to be a proper direction cosine matrix (DCM – a matrix that is both orthonormal and has determinant of +1). In this case the partial derivatives can be expressed as:

$$SS2v(logm(C))_1 C = \begin{bmatrix} a_0 & 0 & 0 \\ 0 & a_0 & -b \\ 0 & b & a_0 \end{bmatrix} \tag{58}$$

$$SS2v(logm(C))_2 C = \begin{bmatrix} a_1 & 0 & b \\ 0 & a_1 & 0 \\ -b & 0 & a_1 \end{bmatrix} \tag{59}$$

$$SS2v(logm(C))_3 C = \begin{bmatrix} a_2 & -b & 0 \\ b & a_2 & 0 \\ 0 & 0 & a_2 \end{bmatrix} \tag{60}$$

where

$$\cos\theta = \frac{trace(C) - 1}{2} \tag{61}$$

$$k = \frac{\theta\cos\theta - \sin\theta}{4\sin^3\theta} \tag{62}$$

$$a_0 = k(C[3,2] - C[2,3]) \tag{63}$$

$$a_1 = k(C[1,3] - C[3,1]) \tag{64}$$

$$a_2 = k(C[2,1] - C[1,2]) \tag{65}$$

$$b = \frac{\theta}{2\sin\theta} \tag{66}$$

and $C[i,j]$ represents entry at the ith row and jth column of C, where 1 represents the first entry.

At this point, we have what is essentially a 3×9 partial derivative matrix that relates how the measurement (z) will change given changes in the estimated C matrix. If we have the derivatives for how C changes given a change in the error states, then we can form our complete H matrix. Using a multiplicative, rather than additive,

39

derivative allows us to find this derivative. First, recall from Equation (30) that the internal matrix is:

$$C_{IMU_r}^{Mag_r} C_{Nav}^{IMU_r} \left(C_{IMU_l}^{Mag_l} C_{Nav}^{IMU_l} \right)^\top \tag{67}$$

Note that this is a valid DCM matrix. To enable changes that still result in a valid DCM, we will take small changes for the right-side IMU as:

$$C_{IMU_r}^{Mag_r} \; expm([v]_\times) \; C_{Nav}^{IMU_r} \left(C_{IMU_l}^{Mag_l} C_{Nav}^{IMU_l} \right)^\top \tag{68}$$

where v is the vector of changes to be applied. (The left-side IMU's DCM is similar but will not be described here.) For small v, this $expm$ expression can be approximated as $I + [v]_\times$. When the derivative is taken this reduces the $expm([v]_\times)$ to just $[v]_\times$. For each element in v, the change in the complete DCM can then be represented as:

$$C_{IMU_r}^{Mag_r} \; SS_j \; C_{Nav}^{IMU_r} \left(C_{IMU_l}^{Mag_l} C_{Nav}^{IMU_l} \right)^\top \tag{69}$$

where $j \in \{1, 2, 3\}$ and

$$SS_1 = \begin{bmatrix} 0 & 0 & 0 \\ 0 & 0 & 1 \\ 0 & -1 & 0 \end{bmatrix} \tag{70}$$

$$SS_2 = \begin{bmatrix} 0 & 0 & -1 \\ 0 & 0 & 0 \\ 1 & 0 & 0 \end{bmatrix} \tag{71}$$

$$SS_3 = \begin{bmatrix} 0 & 1 & 0 \\ -1 & 0 & 0 \\ 0 & 0 & 0 \end{bmatrix} \tag{72}$$

Performing a sum of the element-wise multiplication between the 3×3 matrix

40

for the respective z element and v element gives the partial derivatives necessary to compute H.

In summary,

$$H = \begin{bmatrix} z_1v_1 & z_1v_2 & z_1v_3 \\ z_2v_1 & z_2v_2 & z_2v_3 \\ z_3v_1 & z_3v_2 & z_3v_3 \end{bmatrix} \tag{73}$$

where $\frac{\partial z_i}{\partial v_j}$ is computed by:

1. Computing the current C matrix (Equation (67))

2. Computing $A = SS2v(logm(C))_iC$ using Equations (58)-(60).

3. Using Equation (69), compute matrix B

4. $z_iv_j = \sum_{k=1}^{3} \sum_{l=1}^{3} A[k,l] \cdot B[k,l]$

When a delta rotation has been computed using H, that delta rotation is not added into the error state, but rather because the H matrix computed above does not assume additive error states, changes derived from the Kalman filter (Δr) must change the state as follows [22]:

$$C_{Nav}^{IMU_r+} = expm([\Delta r]_\times)C_{Nav}^{IMU_r-} \tag{74}$$

IV. Results and Analysis

Preamble

To evaluate the effectiveness of each type of measurement, a series of data collection trials of various trajectories were performed. For each trial, the recorded IMU and magnetic sensor data is fed through the algorithm to estimate the trajectory, which is then plotted against the ground truth from GPS readings. For each data run, the results are shown for

- Using the ZUPT update on each IMU individually

- Using the ZUPT and relative rotation updates

- Performing the ZUPT and range updates

- Using all three updates (ZUPT, range, and relative rotation

This breakdown is intended to illustrate the positive, or negative, contribution of the foot-to-foot range and relative rotation measurements extrapolated from the magnetic sensor's position and orientation measurements.

All results were processed using the PDR system with the process noise and measurement noise values of tables 4 and 5. Many of these values were derived from parameter tuning.

Table 5: Measurement Noise Parameters

Name	Notation	Value
ZUPT Measurment Noise	σ_v	0.010 m/s
Relative Rotation Measurment Noise	σ_{rot}	0.400 rad/s
Range Measurement Noise	σ_{range}	0.380 m

4.0.1 Trial 1

The first trial consisted of walk around a residential area. The data capture of each trial begins with an initial period of no movement, with all sensors' data being captured. The stationary period lasts for approximately 20 seconds. The initial data is used to initialize the accelerometer and gyroscope bias calculations as mentioned in section 3.3.1.

The first trial's output in fig. 15a show significant drift effects. While the right foot's estimated path seems to over-commit to turns and curves in the user's trajectory, these features are less effective on the left foot's trajectory.

(a) ZUPT

(b) ZUPT + Rel. Rotation

(c) ZUPT + Range
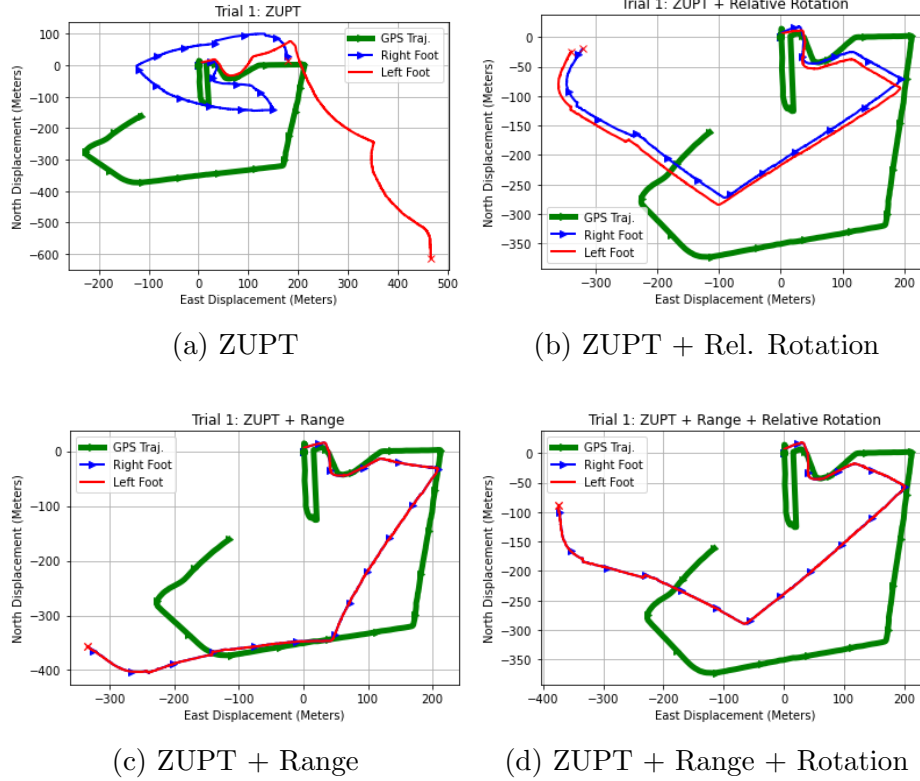
(d) ZUPT + Range + Rotation

Figure 15: Results from trial 1 of pedestrian navigation algorithm with different measurement updates

The addition of the relative rotation measurements to Trial 1 improved the estimated trajectories significantly. Figure 15b shows the effects of coupling the left and

right foot estimates by using the relative rotation technique.

From Figure 15c, the foot-to-foot range measurement tightly couples the left and right estimates trajectories together. The inclusion of this technique also shows greater improvement in accuracy compared to including only the relative rotation measurement with the ZUPT technique. Figure 15d shows the addition of all three measurements. The inclusion of the relative rotation has notable influence on the estimation.

Table 6: Trial 1: ZUPT Error

	Mean	σ
right_x	-24.789	219.444
right_y	-178.555	196.887
left_x	-258.420	263.895
left_y	73.202	162.269

Table 7: Trial 1: ZUPT + Relative Rotation Error

	Mean	σ
right_x	135.455	92.079
right_y	-90.413	121.359
left_x	144.068	96.490
left_y	-81.161	124.194

Table 8: Trial 1: ZUPT + Range Error

	Mean	σ
right_x	89.957	62.528
right_y	37.143	50.628
left_x	90.008	62.613
left_y	37.121	50.574

Table 9: Trial 1: ZUPT + Relative Rotation + Range Error

	Mean	σ
right_x	138.549	93.268
right_y	-64.439	92.031
left_x	138.568	93.317
left_y	-64.501	92.100

4.0.2   Trial 2

The second trial used data captured from a walk around a public park. Figure 16a shows the foot position estimations tracking well, especially in the left foot, until 150 meters down from the starting point.

(a) ZUPT

(b) ZUPT + Rel. Rotation

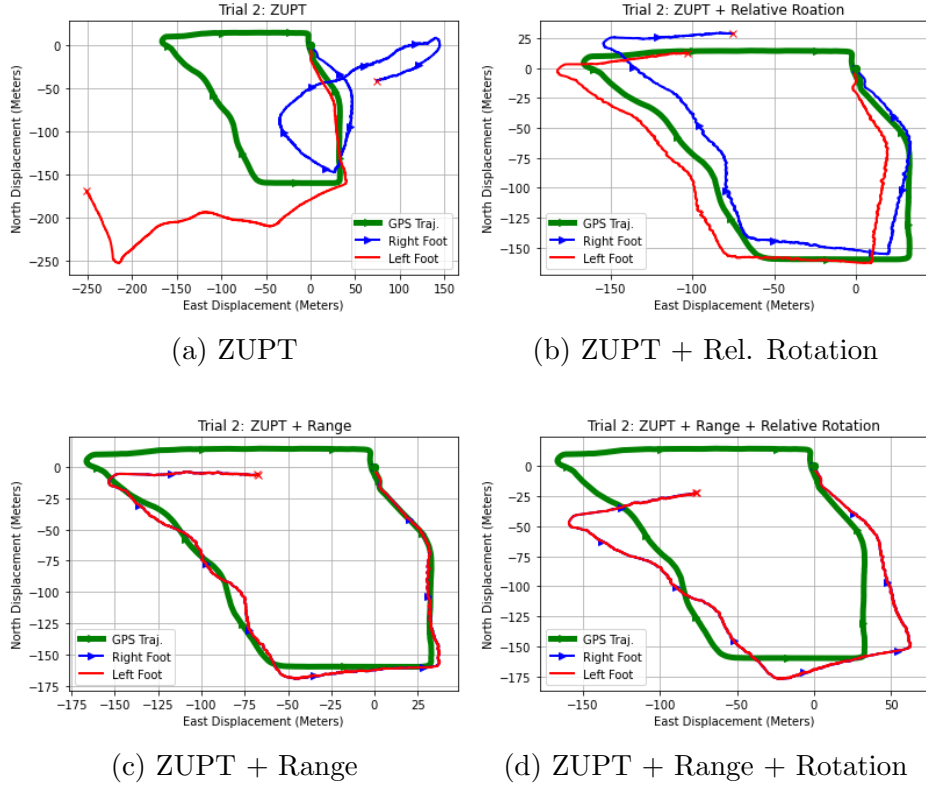(c) ZUPT + Range

(d) ZUPT + Range + Rotation

Figure 16: Results from trial 2 of pedestrian navigation algorithm with different measurement updates

In fig. 16b the relative rotation measurements show improvement to the estimated trajectories. The combination of the foot-to-foot range measurement with the ZUPT

Table 10: Trial 2: ZUPT Error

	Mean	σ
right_x	-97.888	97.573
right_y	-6.678	39.840
left_x	58.027	82.284
left_y	103.501	89.732

Table 11: Trial 2: ZUPT + Relative Rotation Error

	Mean	σ
right_x	5.595	21.454
right_y	-11.508	7.090
left_x	24.621	23.873
left_y	2.018	4.141

Table 12: Trial 2: ZUPT + Range Error

	Mean	σ
right_x	0.131	19.852
right_y	9.618	8.031
left_x	0.043	19.686
left_y	9.635	8.029

Table 13: Trial 2: ZUPT + Relative Rotation + Range Error

	Mean	σ
right_x	-5.518	23.326
right_y	-5.519	7.132
left_x	-5.595	23.273
left_y	-5.484	7.143

technique in Figure 16c has greatly improved accuracy compared to all other measurement combinations in trial 2. The output in Figure 16d also has improvement but shows more offsetting drift errors.

4.0.3 Trial 3

Trial 3 used data captured from a short walk around a house. This trajectory has the shortest distance walked of all the trials, with less than 50 meters total.

(a) ZUPT

(b) ZUPT + Rel. Rotation

(c) ZUPT + Range
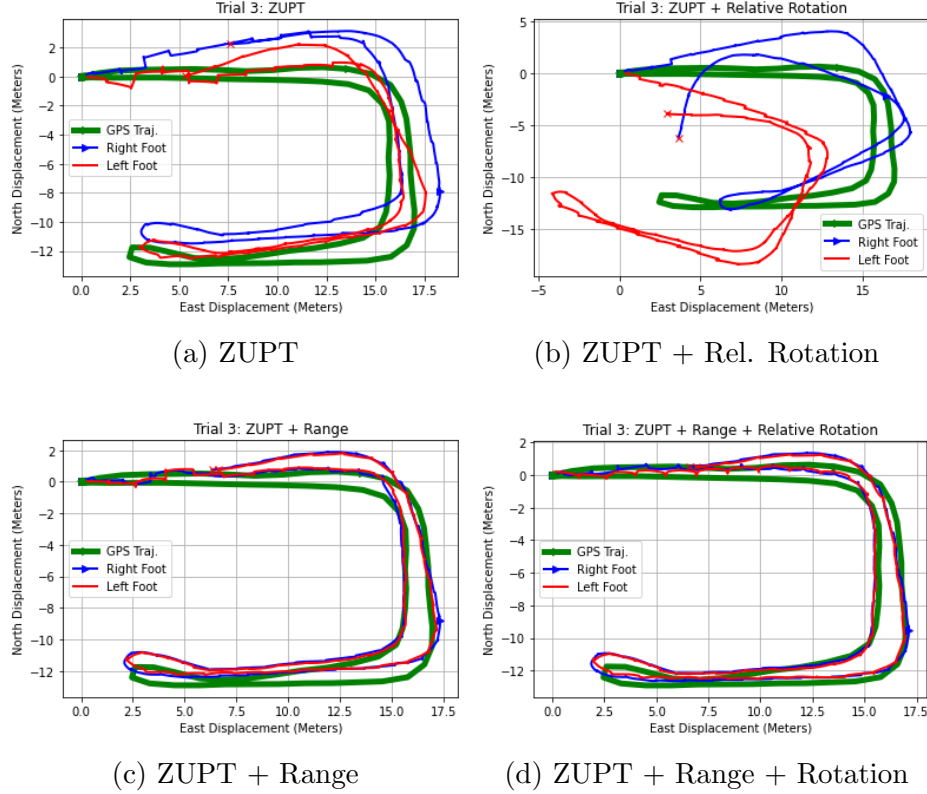
(d) ZUPT + Range + Rotation

Figure 17: Results from trial 3 of pedestrian navigation algorithm with different measurement updates

In fig. 17b the addition of the relative rotation measurement shows a negative effect to the estimated trajectories compared to including the ZUPT measurement alone, fig. 17a.

As the results from section 4.0.1 and section 4.0.2 have shown, the foot-to-foot range measurement with the ZUPT technique in Figure 17c greater accuracy than the relative rotation. The output in Figure 17d has slightly better improvement on accuracy especially on the turns.

Table 14: Trial 3: ZUPT Error

	Mean	σ
right_x	-0.957	1.831
right_y	-1.948	0.848
left_x	-0.277	1.685
left_y	-0.936	1.024

Table 15: Trial 3: ZUPT + Relative Rotation Error

	Mean	σ
right_x	-0.164	3.190
right_y	-0.569	1.503
left_x	4.972	4.152
left_y	3.794	2.867

Table 16: Trial 3: ZUPT + Range Error

	Mean	σ
right_x	-0.244	1.639
right_y	-0.757	0.529
left_x	-0.312	1.694
left_y	-0.770	0.569

Table 17: Trial 3: ZUPT + Relative Rotation + Range Error

	Mean	σ
right_x	2.221	2.839
right_y	2.434	1.725
left_x	2.155	2.929
left_y	2.482	1.699

4.0.4 Trial 4

Trial 4 used data captured from a short walk around a city block.

In fig. 18b the addition of the relative rotation measurement negatively affects the estimated trajectories of the ZUPT measurement alone, fig. 18a, as was also the case in Section 4.0.3.

(a) ZUPT

(b) ZUPT + Rel. Rotation

(c) ZUPT + Range
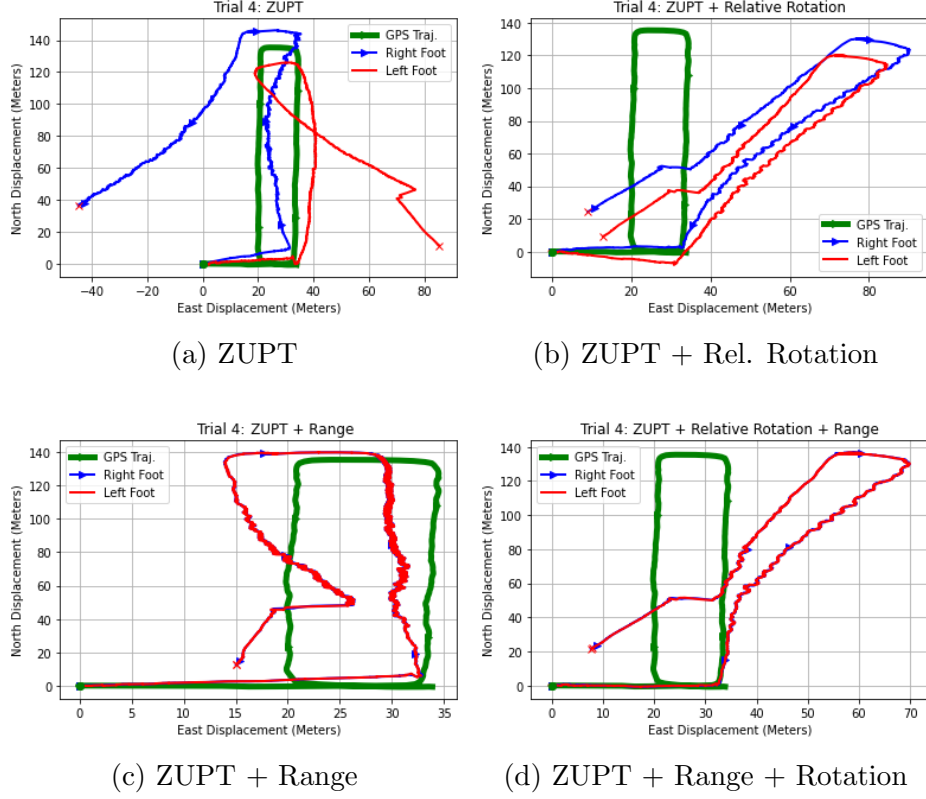
(d) ZUPT + Range + Rotation

Figure 18: Results from trial 4 of pedestrian navigation algorithm with different measurement updates

Staying with the results from each trial, the foot-to-foot range measurement with the ZUPT technique in Figure 18c significantly improves the estimated trajectories compared to the other measurement combinations.

Table 18: Trial 4: ZUPT Error

	Mean	σ
right_x	19.222	22.246
right_y	-11.523	7.746
left_x	-18.817	23.034
left_y	5.275	6.439

Along with a plot of the estimated trajectories. Each iteration of post-process also output a measurement of the average error and standard deviation of the estimates compared to the ground truth. These metrics reflect the observations drawn from

Table 19: Trial 4: ZUPT + Relative Rotation Error

	Mean	σ
right$_x$	-18.451	21.641
right$_y$	-0.810	7.541
left$_x$	-17.873	19.430
left$_y$	10.264	7.111

Table 20: Trial 4: ZUPT + Range Error

	Mean	σ
right$_x$	3.114	3.808
right$_y$	-2.762	3.696
left$_x$	3.116	3.778
left$_y$	-2.803	3.778

Table 21: Trial 4: ZUPT + Relative Rotation + Range Error

	Mean	σ
right$_x$	-9.701	15.059
right$_y$	-2.453	5.290
left$_x$	-9.703	15.048
left$_y$	-2.483	5.407

analyzing the plotted trajectories. The mean errors of the outputs generated using the range measurements show significant decreases to the outputs generated without the range measurements.

Trial 3 in section 4.0.3, with its shorter distance, shows less deviation than the other trials of longer distance. However, as shown in table 14 and table 16, the errors including the relative rotation measurement increases the error compared to the output with only a ZUPT measurement.

V. Conclusions

This thesis reported on the background, objective, methodology, and results of the proposed PDR System. The use of a commercial-grade IMU incorporated with a the Polhemus G4 sensor system, for developing a dual-foot PDR system, have shown promising results. The relative rotation measurement technique shows it can provide significant improvement to a PDR system's ability to accurately estimate a user's trajectory. This new technique did not perform as well as the foot-to-foot range measurement when both are applied with the ZUPT technique.

5.1   Future Work

In Section 3.4.2 we explained the concepts behind the relative rotation measurement. Part of this was the use of a rotation matrix representing the rotation from the IMU to the magnetic sensor on the same foot. While this value should remain constant, as the sensors are mounted to the same case, a future work could involve estimating the rotation along with the other states.

With the introduction of the foot-to-foot range measurement as a technique for improving PDR system accuracy, state observability analysis was conducted to determine the effectiveness of the process [25]. To continue this work, an observability analysis will also be conducted for the relative rotation technique. The intent is that this analysis can shed insight on how ineffective the measurements are in our results.

Another future work to explore is the concept of relative translation measurements. This will also make use of the G4 sensor's unique capabilities.

Add some heavy derivations, extra data and/or plots here.

Bibliography

1. Xinyu Hou and Jeroen Bergmann. Pedestrian dead reckoning with wearable sensors: A systematic review. *IEEE Sensors Journal*, 21(1):143–152, 2021.

2. Oliver J. Woodman. An introduction to inertial navigation. 2007.

3. Jiangbo He, Wu Zhou, Xiaoping He, Huijun Yu, and Longqi Ran. Drift of mems closed-loop accelerometers induced by dielectric charging. *IEEE Transactions on Instrumentation and Measurement*, 70:1–7, 2021.

4. Chi-Shih Jao, Yusheng Wang, and Andrei M. Shkel. Pedestrian inertial navigation system augmented by vision-based foot-to-foot relative position measurements. In *2020 IEEE/ION Position, Location and Navigation Symposium (PLANS)*, pages 900–907, 2020.

5. Michel Laverne, Michael David George, Dale Humbert Lord, Alonzo Kelly, and Tamal Mukherjee. Experimental validation of foot to foot range measurements in pedestrian tracking. 2011.

6. Paul D. Groves. *Principles of GNSS, Inertial, and Multi-sensor Integrated Navigation Systems.* GNSS Technology and Applications Series. Artech House, Inc, 2008.

7. Brian Dunbar. What are passive and active sensors? *NASA*, 08 2017.

8. Polhemus. *G4 User Manual*, 2013. Rev. D.

9. Stefan Hante (https://math.stackexchange.com/users/42060/stefan hante). quot;imaginaryquot; part of a quaternion. Mathematics Stack Exchange. URL:https://math.stackexchange.com/q/3955401 (version: 2020-12-19).

10. David H. Titterton, John, L., and Weston. Strapdown inertial navigation technology - 2nd edition. 2005.

11. Analog Devices. *Data Sheet ADIS16470*, 2017. Rev. C.

12. R.F. Stengel. *Optimal Control and Estimation*. Dover books on advanced mathematics. Dover Publications, 1994.

13. Jordan E Eldridge. Development of a testbed for foot mounted based pedestrian dead reckoning (pdr) systems. Master's thesis, 2021.

14. Greg Welch and Gary Bishop. Welch & bishop , an introduction to the kalman filter 2 1 the discrete kalman filter in 1960. 1994.

15. A.R. Jiménez, F. Seco, J.C. Prieto, and J. Guevara. Indoor pedestrian navigation using an ins/ekf framework for yaw drift reduction and a foot-mounted imu. In *2010 7th Workshop on Positioning, Navigation and Communication*, pages 135–143, 2010.

16. Johann Borenstein, Lauro Ojeda, and Surat Kwanmuang. Heuristic reduction of gyro drift in imu-based personnel tracking systems. *Journal of Navigation*, 62:41 – 58, 01 2009.

17. E. Foxlin. Pedestrian tracking with shoe-mounted inertial sensors. *IEEE Computer Graphics and Applications*, 25(6):38–46, 2005.

18. Sujatha Rajagopal. Personal dead reckoning system with shoe mounted inertial sensors, 2008.

19. Sylvie Treuillet and Eric Royer. Outdoor/indoor vision based localization for blind pedestrian navigation assistance. *Int. J. Image Graphics*, 10:481–496, 10 2010.

20. Raul Feliz, Eduardo Zalama, and Jaime Gómez-García-Bermejo. Pedestrian tracking using inertial sensors. *Journal of Physical Agents*, 3, 01 2009.

21. Carl Fischer, Poorna Talkad Sukumar, and Mike Hazas. Tutorial: Implementing a pedestrian tracker using inertial sensors. *IEEE Pervasive Computing*, 12(2):17–27, 2013.

22. Jenario Johnson and Clark Taylor. Relative magnetic position and rotation sensor assisted dual foot pedestrian dead reckoning. 01 2022.

23. M. Arioli, B. Codenotti, and C. Fassino. The padé method for computing the matrix exponential. *Linear Algebra and its Applications*, 240:111–130, 1996.

24. Honghui Qi and J.B. Moore. Direct kalman filtering approach for gps/ins integration. *IEEE Transactions on Aerospace and Electronic Systems*, 38(2):687–693, 2002.

25. Maoran Zhu, Yuanxin Wu, and Shitu Luo. A pedestrian navigation system by low-cost dual foot-mounted imus and inter-foot ranging. 09 2020.

26. José-Luis Blanco. A tutorial on se(3) transformation parameterizations and on-manifold optimization. Technical report, University of Malaga, September 2010.

Acronyms

BLE Bluetooth Low Energy. 2

GNSS Global Navigation Satellite System. 1

HDR Heuristic Drift Reduction. 17

IMU inertial measurement unit. iv

LCM Lightweight Communications and Marshalling. 22

PDR Pedestrian Dead Reckoning. iv, 20

PNS Pedestrian Navigation System. 1, 18

SLAM Simultaneous Localization And Mapping. 18

WLAN Wireless Local Area Network. 2

ZARU Zero Angular Rate Update. 17

ZUPT Zero Velocity Update. iv, 17

REPORT DOCUMENTATION PAGE

Form Approved
OMB No. 0704–0188

1. REPORT DATE *(DD–MM–YYYY)*	2. REPORT TYPE	3. DATES COVERED *(From — To)*
01–10–2020	Master's Thesis	Oct 2020 — Mar 2022.

4. TITLE AND SUBTITLE

Relative Magnetic Position and Rotation Sensor Assisted
Dual-Foot Pedestrian Dead Reckoning

5a. CONTRACT NUMBER

5b. GRANT NUMBER

5c. PROGRAM ELEMENT NUMBER

6. AUTHOR(S)

Jenario Y. Johnson

5d. PROJECT NUMBER

5e. TASK NUMBER

5f. WORK UNIT NUMBER

7. PERFORMING ORGANIZATION NAME(S) AND ADDRESS(ES)

Air Force Institute of Technology
Graduate School of Engineering and Management (AFIT/EN)
2950 Hobson Way
WPAFB OH 45433-7765

8. PERFORMING ORGANIZATION REPORT NUMBER

AFIT-ENG-MS-22-M-036

9. SPONSORING / MONITORING AGENCY NAME(S) AND ADDRESS(ES)

USA DEVCOM/C5ISR
Daniel A. Dekowski
Building 6007
Aberdeen Proving Ground, MD 21005
Email: daniel.a.dekowski.civ@army.mil

10. SPONSOR/MONITOR'S ACRONYM(S)

DEVCOM/C5ISR

11. SPONSOR/MONITOR'S REPORT NUMBER(S)

12. DISTRIBUTION / AVAILABILITY STATEMENT

DISTRIBUTION STATEMENT A:
APPROVED FOR PUBLIC RELEASE; DISTRIBUTION UNLIMITED.

13. SUPPLEMENTARY NOTES

14. ABSTRACT

The use of wearable foot-based inertial measurement units (IMUs) incorporated in a navigation system can address the problem of single-person location tracking in situations and environments where GPS signals may be unavailable or inconsistent. This Pedestrian Dead Reckoning (PDR) approach enables standalone personal tracking. A notable solution involves using inertial measurement units (IMUs) in a filter to apply zero-velocity updates to a Kalman filter to get a position solution. This paper continues on the path of the former method by investigating the feasibility of PDR using a pair of low cost IMUs along with a pair of relative position and attitude magnetic sensors connected to an individual's feet.

15. SUBJECT TERMS

Pedestrian Dead Reckoning (PDR), Pedestrian Navigation System (PNS), Wearable Technology, Magnetic Sensor, Inertial Measurement Unit (IMU), Filter, Extended Kalman Filter (EKF), Sensor Fusion

16. SECURITY CLASSIFICATION OF:			17. LIMITATION OF ABSTRACT	18. NUMBER OF PAGES	19a. NAME OF RESPONSIBLE PERSON
a. REPORT	b. ABSTRACT	c. THIS PAGE			Dr. Clark Taylor, AFIT/ENG
U	U	U	UU	65	19b. TELEPHONE NUMBER *(include area code)* (937) 255-3636 x4614; Clark.Taylor@afit.edu

Standard Form 298 (Rev. 8–98)
Prescribed by ANSI Std. Z39.18